ChemBioChem

Research Article
doi.org/10.1002/cbic.202400057

Chemistry Europe
European Chemical Societies Publishing

www.chembiochem.org

Nonlinear Impact of Electrolyte Solutions on Protein Dynamics

Hosein Geraili Daronkola[+],[a] Benedikt Söldner[+],[b] Himanshu Singh,[b] Rasmus Linser,*[b] and Ana Vila Verde*[a]

Halophilic organisms have adapted to multi-molar salt concentrations, their cytoplasmic proteins functioning despite stronger attraction between hydrophobic groups. These proteins, of interest in biotechnology because of decreasing fresh-water resources, have excess acidic amino acids. It has been suggested that conformational fluctuations – critical for protein function – decrease in the presence of a stronger hydrophobic effect, and that an acidic proteome would counteract this decrease. However, our understanding of the salt- and acidic amino acid dependency of enzymatic activity is limited. Here, using solution NMR relaxation and molecular dynamics simulations for in total 14 proteins, we show that salt concentration has a limited and moreover non-monotonic impact on protein dynamics. The results speak against the conformational-fluctuations model, instead indicating that maintaining protein dynamics to ensure protein function is not an evolutionary driving force behind the acidic proteome of halophilic proteins.

Introduction

Aqueous environments with NaCl concentrations up to multi-molar are home to halophilic ("salt-loving") organisms. To avoid membrane disruption by high osmotic pressure, many archae halophiles accumulate molar concentrations of KCl in their cytoplasm.[1–3] Cytoplasmic proteins of these organisms, here termed halophilic proteins, hence remain functional and soluble at KCl concentrations far higher than the typical KCl cytoplasmic concentration ($\approx$0.15 mol dm^{-3}) observed in most other organisms on Earth. Proteins (here called mesophilic) of non-halophilic organisms have typically low solubility at molar KCl concentrations.[4–6] Conversely, halophilic proteins often do not remain folded, stable or functional at low KCl concentration.[1,7–10]

Halophilic cytoplasmic proteins contain fewer large + hydrophobic and large + cationic amino acids, but contain more small + polar, small + apolar and acidic amino acids (predominantly at the surface),[8] than mesophilic proteins.[7,9,11] As a result, halophilic proteins have higher net negative charges than mesophilic ones (an average of $-8e$ to $-10e$ vs. $-1e$ to $-3e$, respectively).[9] Multiple hypotheses have been advanced to explain this difference, via the impact it will have on protein solubility (i.e., propensity for protein aggregation), thermodynamic stability of the folded protein conformation, and biological function of the molecule (e.g., enzymatic activity). Prior work has focused on clarifying the impact of acidic amino acids and salt on protein solubility and on the thermodynamic stability of folded proteins.[12] In contrast, our understanding of the mechanism(s) leading to strong salt dependency of enzymatic activity – a dependency that is often different from the salt-dependency of protein aggregation and protein conformational stability – and the eventual contribution of acidic amino acids to this dependency, is limited.

A key player in enzymatic activity is enzyme flexibility, defined as the amplitude and frequency of fluctuations in conformation experienced by the folded enzyme.[13–16] Higher protein flexibility is more often associated with motions of higher amplitude but may also be associated with faster motions (of the same amplitude). Enzyme activity involves physical steps necessary to bring substrates and cofactors to their binding sites and to release the product, as well as the chemical step itself.[17] Whereas the direct relation between enzyme flexibility and the chemical step is not fully elucidated, experimental and simulation studies have clearly demonstrated a connection between enzyme flexibility and the physical steps.[17,18]

According to the conformational-fluctuations model, the increased magnitude of the hydrophobic effect at high salt concentrations would decrease protein flexibility relative to lower salt concentrations.[19] In this scenario the increased intramolecular repulsion brought by the acidic proteome of halophilic proteins helps maintaining conformational fluctuations key for function at high salt concentration.[19] Studies of a limited number of non-halophilic proteins have suggested that a decrease in enzyme function correlates with increased

[a] Dr. H. G. Daronkola,[+] Dr. A. V. Verde
University of Duisburg-Essen, Faculty of Physics,
47057 Duisburg, Germany
E-mail: ana.araujo-vila-verde@uni-due.de

[b] B. Söldner,[+] Dr. H. Singh, Prof. Dr. R. Linser
Technical University Dortmund,
Faculty of Chemistry and Chemical Biology,
44227 Dortmund, Germany
E-mail: rasmus.linser@tu-dortmund.de

[+] These authors contributed equally.

Supporting information for this article is available on the WWW under https://doi.org/10.1002/cbic.202400057

thermodynamic stability in some cases, and that this correlation arises because of a reduction of protein flexibility.[14] To date, however, a comprehensive assessment of how protein structural flexibility responds to changes in salt concentration, whether that response differs between halophilic and mesophilic proteins, and the role of charged amino acids in this response does not exist.

Here we use NMR, molecular dynamics (MD) simulations, and analytical models to understand how protein structural flexibility is affected by the concentration of KCl. Simulations are performed on 5 pairs of halophilic and mesophilic proteins, and experiments are performed on 4 mesophilic proteins. Covering a wide range of sizes, net charges, and degrees of flexibility at their native electrolyte concentration, generalized conclusions on the dependency of flexibility on changes in salt concentration and the role of acidic amino acids in halophilic adaptation are obtained.

Results

Experimental Results

We first probed protein motion as a function of KCl concentration within four different – ^{15}N- or ^{15}N/^{13}C-labeled – mesophilic proteins with a molecular-weight range between 7 kDa and 42 kDa using NMR spectroscopy in solution. In particular, we targeted the SH3 domain of chicken α-spectrin (7.4 kDa), ubiquitin (8.5 kDa), human carbonic anhydrase (29 kDa), and maltose binding protein (42 kDa). The first two proteins are small but contain all different forms of secondary-structural motifs; a very high signal-to-noise can be achieved. The last two proteins are reasonably complex structures with sizeable hydrophobic cores.

To comprehensively capture changes in protein flexibility as a function of salt concentration, we turned to experiments addressing two different time regimes. Fast (ps-ns timescale) motion was targeted using the [^{15}N, ^{1}H] heteronuclear nuclear Overhauser effect (hetNOE). hetNOE values approach 1 for rigid amino acids whereas values down to zero, sometimes lower, are found for very flexible elements of the protein primary sequence. The latter case is a representative of substantial fast (ps-ns) timescale fluctuations of the ^{1}H-^{15}N bond vector, with decreasing values both for faster and for higher-amplitude motion (lower order parameters). Figure 1(A, B) show the hetNOE values of the SH3 domain and of hCAII, respectively, as a function of residue number, for no-salt and high-salt conditions. For SH3, several local differences are observed with and without KCl, but no global changes are apparent. With addition of KCl, hetNOE values of the N-terminus, 28Gly and 41Trp are slightly reduced, indicating slightly increased mobility on the pico- to nanosecond timescale, while hetNOE values are strongly increased for 38Asn (n-Src loop, from 0.079 to 0.813) and 47Asn (distal loop, from 0.097 to 0.725), indicating a considerable rigidification in the ps-ns timescale regime upon addition of KCl. In case of hCAII, hetNOE values increase for several residues upon addition of salt (e.g. residues 55–57, 59, 62, 92–94, 96 and 106–107), however, no global shift is visible. As the highest hetNOE values are expected to be uniform among the rigid residues and are defined by the overall tumbling correlation time, the outliers are likely due to a higher degree of uncertainty. hetNOEs for ubiquitin and MBP are shown as a function of residue number in Figure S2, where similar trends can be observed.

To assess global differences of hetNOE between low and high concentration of KCl, the sequential plots of all four proteins were statistically analyzed using box plots (Figure 1C). In these plots the region between the first and third quartile is depicted as a box. Figure S3 depicts the same data in the form of a histogram. For SH3 and ubiquitin, the average of hetNOE values for the 3 secondary structure categories investigated are very close to 1, indicating that these proteins are not very flexible in the ps-ns time scale. The distributions of hetNOE values are very narrow, especially for α-helical and β-sheet-like secondary structural regions. Box sizes and median values are virtually identical at low and high salt concentration, revealing no impact of salt concentration on dynamics of SH3 and ubiquitin. For hCAII and MBP, more hetNOE values deviate from 1, indicating that these proteins bear more flexible residues. Moreover, hetNOE values are much more dispersed at 2.0 M KCl concentration, which may reflect some impact of salt on the flexibility of these proteins but at least in part derives from the decreased sensitivity of the measurements under high-salt conditions. In agreement with the latter, despite the larger distributions, the median hetNOE values for the three secondary structure categories analysed here remain untouched by the high salt concentration. Overall, the hetNOE data show that changes in salt concentration have either no impact or only minor impact on protein dynamics, these effects being more pronounced for protein regions with higher mobility compared to those that are motionally restricted. The dependence of protein flexibility on salt concentration, whenever present, is not systematic: we observe both increases and decreases in residue flexibility with increasing salt concentration. Similar trends are observed in our chemical-shift perturbation study, described in section S2.2.

We investigated protein dynamics at a slower (μs-ms) timescale using Carr-Purcell-Meiboom-Gill (CPMG) relaxation dispersion measurements. These quantify the excess contribution (R_{ex}) to the transverse relaxation rate R_2 that arises for a ^{15}N nucleus through sampling of differential isotropic chemical shifts upon conformational exchange. R_{ex} increases as the population of the minor state increases and as the difference in chemical shifts between the conformations increases. Whereas such measurements can also inform on conformational-exchange timescales and even populations, in this work we restrict our interpretation of differences in R_{ex} between two salt concentrations as indicating a different extent of conformational exchange. Note that caution has to be taken when interpreting relaxation dispersion data for different buffers due to their impact on the chemical shifts of ground and excited-state conformations.[21–23]

Figure 2(A, B) show the R_{ex} rates for the proteins ubiquitin and MBP. For ubiquitin, which shows an overall extremely low

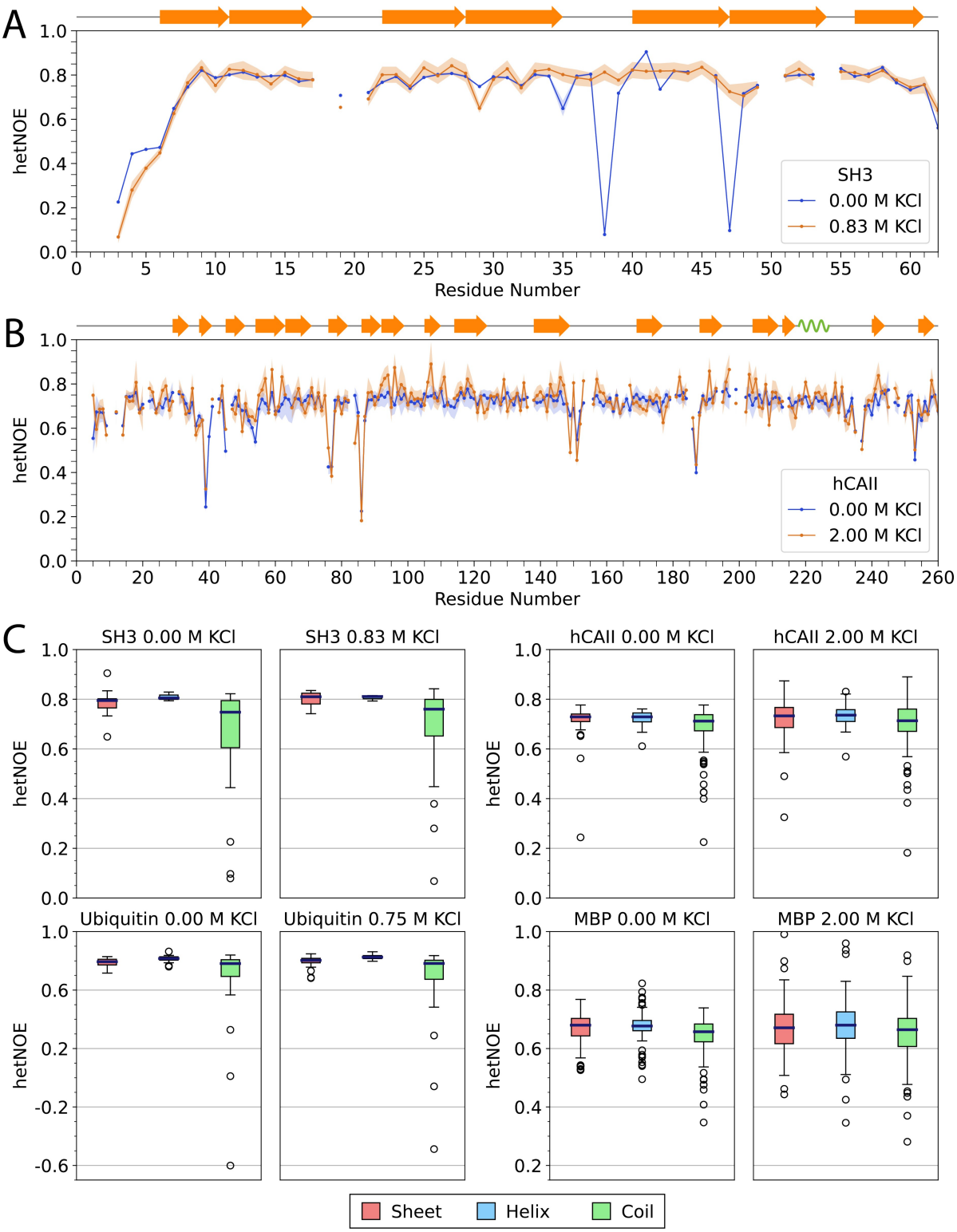

Figure 1. Picosecond to nanosecond timescale motion with and without KCl, as measured by [^{15}N, ^{1}H] heteronuclear nuclear Overhauser effect, defined as the ratio I_{sat}/I_{eq}, where I_{sat} and I_{eq} are the intensities of peaks in the 2D experiments with and without proton saturation, respectively. (A) hetNOE of the SH3 domain of chicken α-spectrin as a function of residue number. (B) hetNOE of human carbonic anhydrase II. The shaded areas around the curve represent the propagated error estimated from the spectral noise as described in the Methods section. (C) Distribution of hetNOE values (box plots) in the proteins SH3, ubiquitin, hCAII, and MBP for different secondary structure motifs. Note the experimental intricacies of determining precise NOE values for high-molecular-weight proteins.[20] Boxes extend from the first to the third quartile with a line at the median. The whiskers extend over 1.5× the inter-quartile range from the box. Outliers are marked as white circles. All means and distributions are highly similar between no-salt and high-KCl conditions.

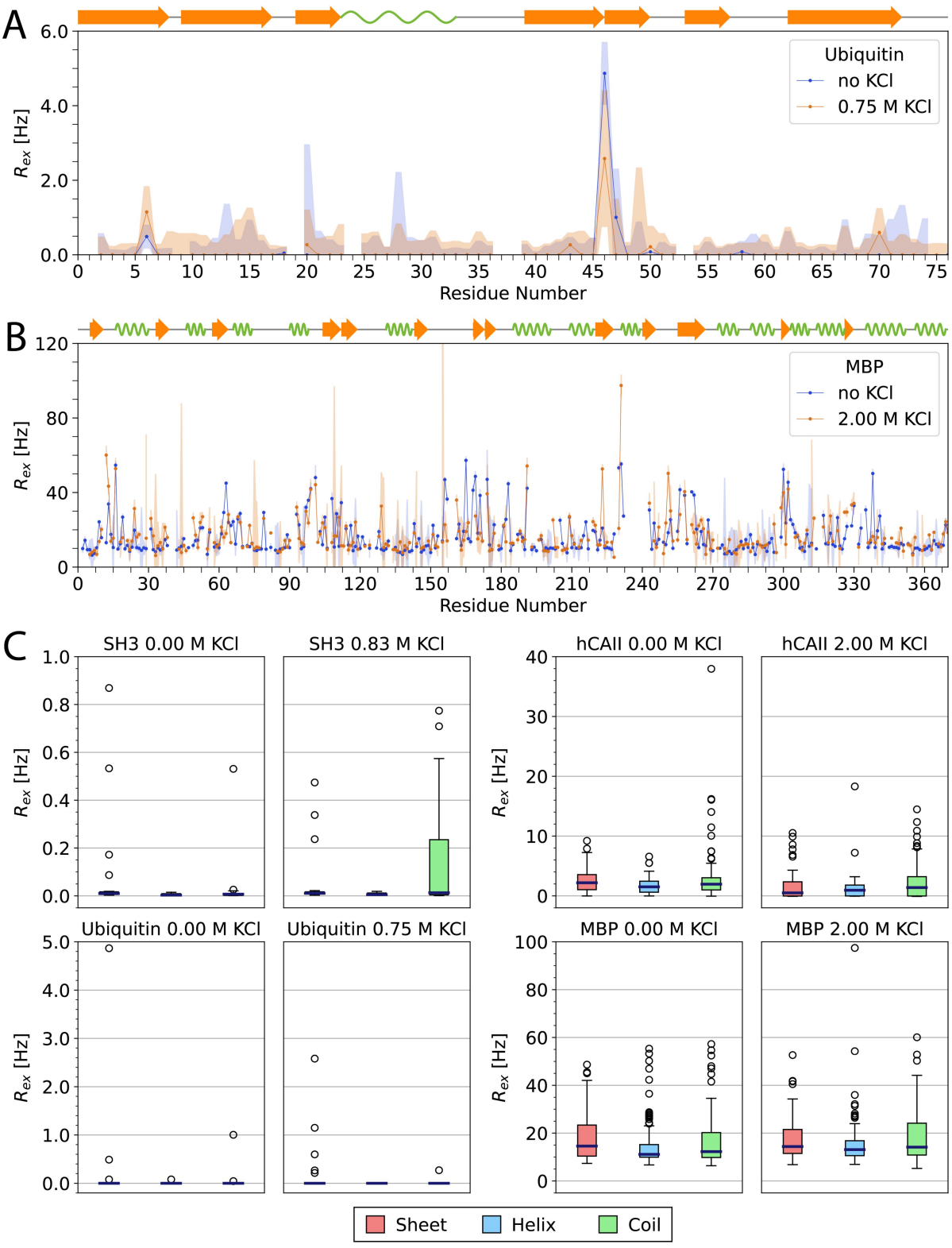

Figure 2. Microsecond to millisecond timescale motion, represented by the exchange contribution R_{ex} extracted from CPMG relaxation dispersion experiments. (A) Residue-specific R_{ex} in ubiquitin, (B) residue-specific R_{ex} in MBP. The shaded areas around the curve represent the propagated error estimated from the spectral noise as described in the Methods section. (C) Distribution of R_{ex} values (box plots) in the proteins SH3, ubiquitin, hCAII, and MBP, for different secondary structure motifs. The meaning of each symbol is described in Figure 1.

extent of motion at the µs-ms timescale, no significant alterations for exchange rate values are observable between the two salt concentrations. Likewise, even though MBP displays a larger range of slow motions than ubiquitin, system-

atic changes in dynamics with salt concentration over the entire protein are also not observed. The higher degree of fluctuations observed for MBP at the high-salt condition likely derives from measurement uncertainties; the standard deviation of the R_{ex} values over the entire protein is 10.5. Several residues show a higher exchange contribution at low salt (e.g., residues 62, 63 and some between 150 and 175; blue). In contrast, other residues show a higher exchange contribution at high salt (e.g., residues 12, 13, 223, 251). However, no clear connection between the structural motif in which these residues are embedded or their extent of surface exposure is discernible. Figure S4 shows the R_{ex} rates as a function of sequence for the remaining proteins SH3 and hCAII under no-salt and high-salt conditions. Similarly to MPB and ubiquitin, SH3 and hCAII do not show global changes in dynamics with salt concentration, with only a few residues in hCAII showing statistically different values of R_{ex} between the two salt concentrations.

We statistically assessed the distributions of all four proteins again in the form of box plots (Figure 2C). For SH3 and ubiquitin, the distributions of R_{ex} rates are again very small. Apart from a minor change in the average R_{ex} rates for β-sheet-like secondary structure elements in hCAII with salt concentrations, the box plots show no significant changes in R_{ex} rates with salt concentration. The histograms of exchange contributions (Figure S5) of hCAII and MBP differ quantitatively between the two salt conditions whereas those for ubiquitin and for SH3 are practically identical. Nevertheless, a systematic impact of salt on the dynamics of particular structural motifs or on the dynamics of the whole protein is not found for any of the 4 proteins.

Simulation

To investigate how atomic fluctuations respond to salt concentration and the potential role of acidic amino acids in the maintenance of protein flexibility at high salt concentration, we performed atomistic MD simulations comparing 5 halophilic proteins with their mesophilic counterparts. An illustrative simulation box is shown in Figure 3; names and pdb IDs given in Figure 4. Each halophilic-mesophilic pair was selected to ensure high similarity in amino acid sequence and structure between the two proteins while having a wide range of sizes and net charges in each category, as discussed in section S1.1. This diverse and representative group of proteins enables us to generalize conclusions based on our observations.

Each protein was simulated in aqueous KCl solutions with molality $b_{KCl} = 0.15\ mol\,kg^{-1}$ and $b_{KCl} = 2\ mol\,kg^{-1}$. The high salt concentration is thus non-optimal for the mesophilic proteins; the low salt concentration is likewise non-optimal for the halophilic ones. In section S2.4.1 we show that the protein structures remain stable during the entire simulation time.

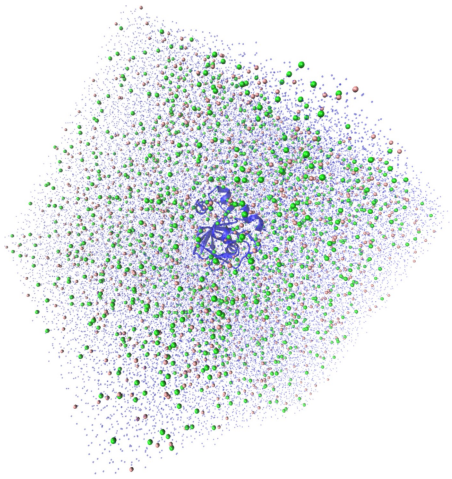

Figure 3. Example simulation box, of the halophilic ferredoxin protein (pdb ID: 1DOI). Dark blue shape = New Cartoon representation of protein; Pink spheres = K^+; Green spheres: Cl^-; Transparent small blue dots: water molecules.

Conformational Flexibility

The Root Mean Square Fluctuation (RMSF) quantifies the amplitude of atomic displacements relative to the average position, as detailed in section S1.3.4. Figure 4 shows the RMSF per residue (heavy atoms only) of each protein, at high and low salt concentration; Figure S7 shows the same data in histogram form. Similarly to what was observed in the hetNOE values and R_{ex} rates, different protein sections and even adjacent residues in the protein sequence can have dramatically different dynamics. Increasing salt concentration impacts protein flexibility only locally, for protein residues that show high flexibility (as measured by RMSF larger than 2 Å) at low salt concentration, which are predominantly found in coil structure (Figure S8). The majority of flexible protein sections (found in proteins 2L28, 2ITH, 1FRD, 1HZ6 and 4CNX) becomes less flexible at high salt concentration. The opposite salt dependency is also seen, but more rarely: some sections of the mesophilic proteins 1V9E and 2L28 and of the halophilic protein 3WRT show larger RMSF at higher salt concentration. In contrast, the dynamics of residues without large-amplitude motions is only marginally sensitive to salt concentration; this weak dependence is easily seen in the RMSF histograms (Figure S7) of proteins 1ZKJ, 3WRT, 2KAC and 1V9E. These results are in line with a prior computational study of a ubiquitin-like protein,[24] a neutron scattering study of bovine serum albumine,[25] and with our NMR experiments discussed above.

Mechanism of Flexibility Modulation by Salt

To understand the origin of the non-monotonic effect of salt on protein dynamics, we consider the impact of salt concentration on the hydrophobic effect and on electrostatics. We consider

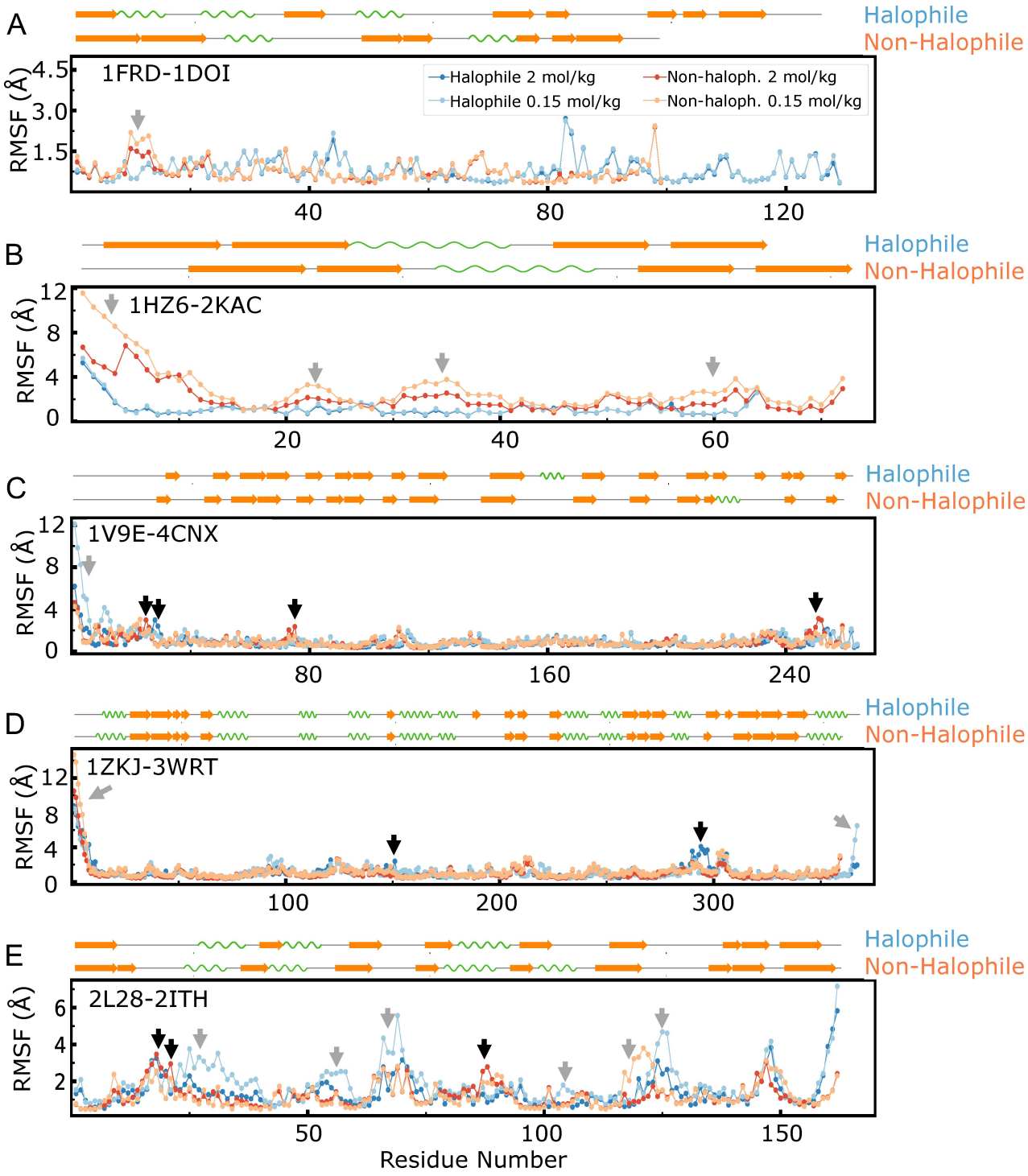

Figure 4. RMSF of each residue of the indicated mesophilic-halophilic protein pairs, at high and low KCl concentration, calculated from MD simulation. (A) ferredoxin; (B) protein L; (C) carbonic anhydrase; (D) β-lactamase; (E) dihydrofolate reductase. Black arrows point to some of the residues for which the RMSF of a protein is higher at the high salt concentration; grey arrows point to some of the residues for which the RMSF is higher at the low salt concentration.

only salts without strong specific interactions with protein charged groups, as is the case for KCl.[26]

The Hydrophobic Effect and Protein Flexibility

Figure 5(A) shows normalized hydrophobic solvent accessible surface area (SASA) histograms, *P*(*A*), for two of the proteins, obtained from simulation; the histograms for the other proteins are shown in Figure S9. The SASA distributions are mono-

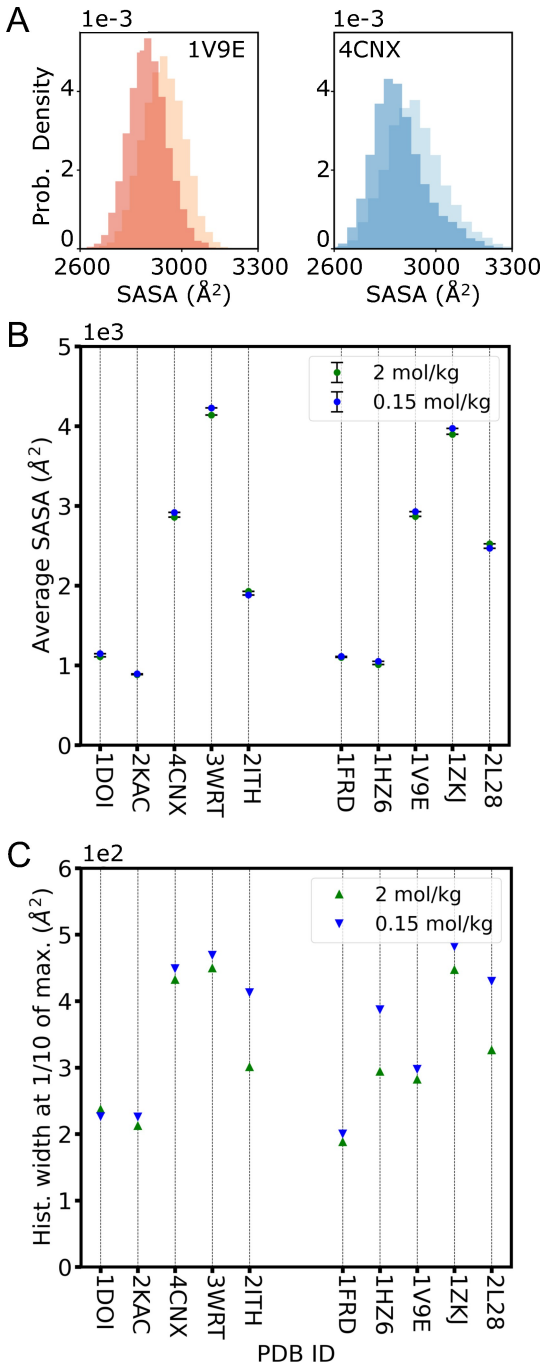

Figure 5. Hydrophobic SASA associated with hydrophobic residues, at high and low salt concentration, calculated from MD simulation: (A) Illustrative histograms for the proteins with the indicated pdb IDs, at $b_{KCl} = 2$ mol kg^{-1} (dark blue and orange) and $b_{KCl} = 0.15$ mol kg^{-1} (light blue and orange); protein 4CNX is halophilic and protein 1V9E is mesophilic; (B) SASA mean; the error bars show the standard error of the mean; (C) Histogram width at 1/10 of maximum height. Differences below 50 Å^2 are not statistically significant.

peaked and show little or no skewness, so the distributions can be characterized by their mean and width. Figure 5(B) shows the mean hydrophobic SASA of the proteins studied in simulation; numerical values are shown in Table S4. The mean hydrophobic SASA varies between 1000 Å^2 and 4000 Å^2. For 8 of the 10 proteins studied here, the hydrophobic SASA is lower at high salt concentration, by between 10 Å^2 and 60 Å^2. Only the proteins 2L28 and 2ITH have higher mean hydrophobic SASA, by ≈60 Å, at the higher salt concentration. For either type of response, the mean hydrophobic SASA of each protein at the two salt concentrations differs less than the surface area of a single methane molecule, indicating that the mean hydrophobic SASA depends only weakly on salt concentration. But, what is the impact of salt on hydrophobic SASA fluctuations?

We quantify SASA fluctuations through the width of the histogram at 1/10 of the histogram maximum. Figure 5(C) indicates that the width of the hydrophobic SASA histograms is very weakly reduced at high salt concentration for seven of the 10 proteins studied. Only for three of the proteins – the halophilic 2ITH and the mesophilic 2L28 and 1HZ6 – does the hydrophobic SASA histogram become markedly narrower at high salt concentration. These results correlate well with the salt-dependent RMSF values presented above, in which proteins 1HZ6, 2ITH and 2L28 show the strongest salt-dependent flexibility.

To understand the extent to which changes in SASA fluctuations with salt concentration can be explained by the hydrophobic effect, we take the commonly used approximation[12,27] that the free-energy cost (ΔG_{cav}) of introducing an apolar group in aqueous solution scales linearly with the surface tension (γ) of the solution and with the area, A, of the group according to:

$$\Delta G_{cav} = \gamma \times A \tag{1}$$

The impact that a change in salt concentration has on the fluctuations in hydrophobic SASA via a change in the hydrophobic effect can be estimated from Eq. (1) and from the probability density, $P_{ref}(\Delta A)$, of those fluctuations at a reference salt concentration, as:

$$P_c(A) = D_2 P_{ref}(A) \exp\left(-\frac{\Delta\gamma A}{k_B T}\right) \tag{2}$$

where $P_c(A)$ is the probability density of the SASA fluctuations at the new salt concentration, $\Delta\gamma = \gamma_c - \gamma_{ref}$ is the difference of the surface tension at the two concentrations, T is the temperature, k_B is the Boltzmann constant and D_2 is a normalization constant (see section S2.4.3 for further details).

Figure 6 shows distributions of hydrophobic SASA obtained through this model. Modifying that reference distribution according to Eq. (2) for estimates of $\Delta\gamma$ between 0.15 mol kg^{-1} and 2 mol kg^{-1} leads to the $P_c(A)$ curves shown in blue when considering macroscopic values of the surface tension of electrolyte solutions, and in orange when considering that the microscopic surface tension is roughly half of the macroscopic one.[12,28] The increased hydrophobic effect systematically lowers the mean hydrophobic SASA by 40 Å^2 when using microscopic γ values, and by 100 Å^2 when using macroscopic γ values. The decrease in mean hydrophobic SASA at high salt concentration

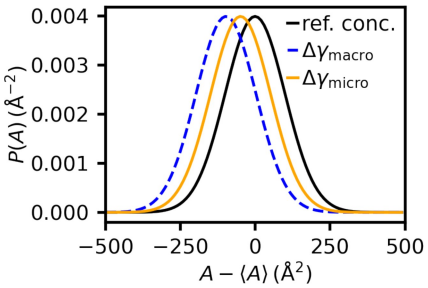

Figure 6. Probability density distribution of hydrophobic SASA at $b_{KCl}=2$ mol kg^{-1} considering macroscopic ($\Delta\gamma_{macro}$) and microscopic ($\Delta\gamma_{micro}$) values of surface tension, predicted through Eqs. (1) and (2), given a model $P_{ref}(A)$ at the reference concentration modelled as a normal distribution with mean $\langle A\rangle$ and standard deviation 100 Å^2. $\Delta\gamma_{micro}=0.5\,\Delta\gamma_{macro}=0.5\times(76-72)$ mN m^{-1}.[12,28,29]

predicted by this model is consistent with simulation results for 8 of the 10 proteins investigated here (see Table S4).

The model also predicts that salt concentration has no impact on the amplitude of the hydrophobic SASA fluctuations relative to the mean. This response occurs because the energetic penalty associated with changes in salt concentration depends linearly on *A*. This simple model suggests that the enhanced hydrophobic effect at high salt concentration will not impact protein flexibility as measured by the width of hydrophobic SASA fluctuations, although it will slightly reduce the mean hydrophobic SASA, consistent with the results in Figure 5(B). It follows that the narrowing of the width of the SASA histograms of proteins 2ITH, 1HZ6 and 2L28 must be the result of other mechanisms.

Electrostatic Interactions and Protein Flexibility

We consider two elementary charges as a model of charged amino acids in a folded protein. In the simulation environment these charges will be under the influence of multiple other potentials (bond, angle, dihedral, Lennard-Jones potentials, electrostatic interactions with other charges). The impact of these interactions on the inter-charge distance is implicitly captured by the distribution, $P_{ref}(r)$, of inter-charge distance at a reference salt concentration, and is assumed to be independent of salt concentration. Applying a formalism analogous to that used to model the hydrophobic SASA fluctuations, the distribution of inter-charge distance, $P_c(r)$, at a given salt concentration *c* can be estimated from $P_{ref}(r)$ by considering the impact that the change in salt concentration has on the electrostatic interactions between the two charges in question:

$$P_c(r) = E\exp\left[-\frac{U_{electr,c}(r)-U_{electr,ref}(r)}{k_BT}\right]P_{ref}(r) \qquad (3)$$

E is a normalization constant and $U_{electr}(r)$ is modelled through the Debye-Hückel theory. The salt dependence of electrostatic interactions is present in the salt-dependent values of the relative permittivity of the electrolyte solution and of the Debye length. Further details are given in section S2.4.4.

Figure 7 shows predictions from Eq. (3). The reference distributions are modelled as asymmetric potentials because the inter-charge distance cannot be smaller than the van der Waals radius of atoms. Panel A.i shows predictions when the distance distribution at the reference concentration is narrow and thus does not allow substantial fluctuations. In this case, increasing salt concentration barely impacts the inter-charge distance, reflecting the fact that the other interactions affecting the charges are much more intense than their electrostatic interaction. In panel A.ii we show the response of the fluctuations if the two charges have magnitude 2*e*, as an approximation to the scenario of a pair of charged amino acids interacting with a nearby pair of charged amino acids. In this case, the distribution of inter-charge distances responds, albeit still weakly, to the change in salt concentration. Because of stronger charge screening at high salt concentration, like-charges on average come closer together *and* they experience narrower fluctuations around the new mean distance. In contrast, unlike-charges on average move further apart and fluctuate more amply around the new mean distance.

The scenario of charges under the influence of a soft potential, with FWHM ≈5 Å, is examined Figure 7B. Panel B.i shows predictions for single point charges. Distance fluctuations now clearly reflect an impact of salt concentration, with unlike-charges substantially increasing the range of their distance fluctuations as salt concentration increases and like-charges showing the opposite behavior. Panel B.ii clarifies that changes in fluctuations in response to salt concentration become dramatically more intense, for both like and unlike charges, when the two charges have magnitude 2*e*.

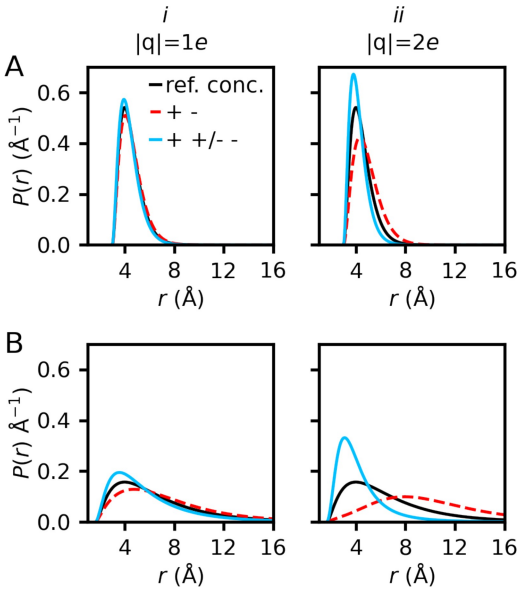

Figure 7. Probability density distribution of inter-charge distance fluctuations at 2 mol kg^{-1} (blue and dashed red curves) predicted through Eq. (2) from $P_{ref}(r)$ (black curve) at the reference concentration $b_{KCl}=0.15$ mol kg^{-1} for (A) narrow and (B) wide model $P_{ref}(r)$ distributions, for (*i*) mono and (*ii*) divalent charges.

The results from these analytical models qualitatively explain both the salt-dependent and the salt-independent protein dynamics observed in simulations and experiment, as illustrated in Figure 8. Only minimal changes in *global* protein flexibility with salt concentration are seen for many folded proteins because they are rigid. In this case, changes in the magnitude of the hydrophobic effect or of electrostatic interactions remain small relative to the other interactions governing protein flexibility, so flexibility changes little with salt concentration; this is seen in the small changes (<100 Å^2, less than one methane molecule) in the width of the hydrophobic SASA histograms as a function of salt concentration experienced by all proteins investigated in simulation (Figure 5). The hydrophobic effect can strongly reduce the flexibility of flexible protein sections that contain some hydrophobic amino acids and are exposed to solvent (orange arrow in Figure 8; hydrophobic amino acids not shown). More often, however, a strong reduction in local protein flexibility is associated with protein regions rich in like-charges, which at high salt concentration no longer strongly repel (black arrows in Figure 8). Likewise, a strong local increase in protein flexibility at high salt concentration may also occur when stabilizing salt bridges at low salt concentration become screened at high salt concentration (red arrows in Figure 8).

Concluding Remarks

Our results demonstrate that changes in salt concentration barely impact the dynamics of rigid protein sections, but may noticeably impact the dynamics of flexible protein regions. The stronger hydrophobic effect at high salt concentrations has limited bearing on the flexibility of folded proteins, contrary to expectations.[14,19] Instead, changes in salt concentration influence protein flexibility primarily through electrostatics. As salt concentration increases, flexible protein regions rich in like-charges will experience an increase in low-amplitude motions because charge screening will enable the protein to explore conformations where the charges come closer together, at the expense of expanded conformations. We note that lower-amplitude motions may manifest as an enhancement in *short* time-scale dynamics, because low amplitude motions are typically faster. An enhancement of fast dynamics at high salt concentration has been reported from neutron scattering experiments on tRNA.[30,31] By contrast, flexible regions rich in unlike-charges may increase the amplitude of their motions when salt concentration increases because of screening of salt bridges at high salt concentration.

Our results do not support the scenario that an enrichment in acidic amino acids and the corresponding high negative net charge is necessary to ensure protein flexibility in a halophilic environment.[32] More likely, excess acidic amino acids are involved in other mechanisms that enable halophilic proteins to function at high salt concentration, such as reduction of hydrophobic solvent-accessible surface area,[33] preferential solvation of the folded state,[32,34–36] cooperative carboxylate-cation-water networks[32,37] or prevention of aggregation.[33,36,38–40]

Our results identify which physical information must be considered to efficiently predict protein conformational ensembles and protein dynamics as a function of salt concentration. They also highlight the complex and non-linear interplay between all factors contributing to protein dynamics, which makes it difficult to predict it using simplified physical models. Strong predictive capabilities may be more easily obtained with machine learning,[41] which can efficiently handle non-linearities, in particular physics-informed machine learning approaches[42] which can incorporate the physical insights revealed here. The beneficial impact of these insights on future predictions will be critical to guide the modification of biotechnologically useful enzymes[43–46] so they can remain functional in saline solutions thus reducing dependency on our fresh water resources, to obtain improved understanding of the connection between salt-dependent protein dynamics and protein-protein interactions in the course of evolution,[47–50] and to foster improved strategies for formulations of protein pharmaceutics and in structural biology.

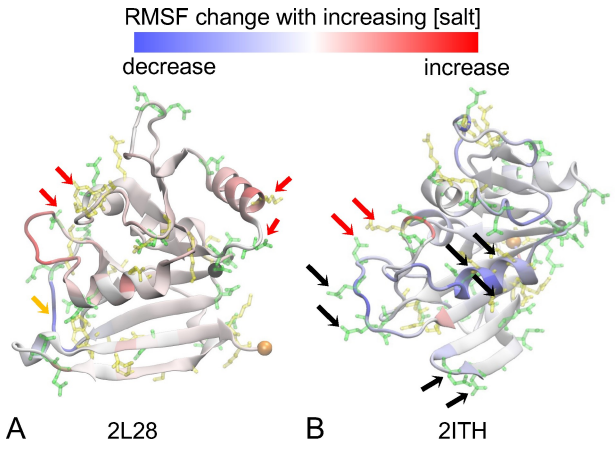

Figure 8. Local change in protein flexibility (ΔRMSF), as measured by the difference in the RMSF values of each amino acid (i) at high and low salt concentration ($\Delta RMSF(i) = RMSF_{2m}(i) - RMSF_{0.15m}(i)$; values from Figure 4), for the (A) mesophilic and (B) halophilic dihydrofolate reductase proteins investigated in simulations. The blue-white-red color scale indicates a reduction-maintenance-increase in protein flexibility with increasing salt concentration. Green = acidic amino acids; yellow = basic amino acids; grey, orange spheres = amino acid termini. Red and black arrows indicate unlike-charge/like-charge interactions that are screened at high salt concentrations and contribute to positive/negative values of ΔRMSF, respectively. The orange arrow indicates a negative ΔRMSF likely resulting from an increase in the hydrophobic effect.

Experimental

Experimental Methods

Proteins Used for NMR Spectroscopy

Nuclear magnetic resonance (NMR) experiments were performed on 4 proteins: α-spectrin SH3 domain (SH3), ubiquitin, human carbonic anhydrase II (hCAII), and maltose binding protein (MBP). All proteins were purchased from Giotto Biotech, Italy. Table S1 lists

the pdb IDs and amino acid content of each protein, and Table S2 details the experimental conditions used for each protein.

NMR Sample Preparation and Measurement

For NMR studies, uniformly ^{15}N or $^{13}C/^{15}N$-labeled protein samples were prepared in a mixed solvent of 90% $^{1}H_2O$ and 10% $^{2}H_2O$ (sample conditions summarized in Table S2). All NMR experiments were carried out with protein concentrations of 0.5 mM on a Bruker Avance 800 MHz NMR spectrometer equipped with a 5 mm cryogenically cooled triple-resonance probe and a pulse-field gradient. The ^{1}H, ^{15}N resonance assignments of SH3, ubiquitin, hCAII and MBP proteins were taken from the Biological Magnetic Resonance Bank (BMRB, accession numbers 34420, 1541, 34308 and 4986, respectively). In the case of MBP, assignments were further completed using a 3D HNCA triple-resonance experiment. Chemical shifts for high-salt conditions were obtained using a titration approach, upon which original H/N HSQC or HNCA peaks could be tracked upon increase of KCl concentrations and associated with their new positions. Further protein preparative procedures and experimental conditions are given in section S1.2.

Chemical-Shift Perturbations

Chemical-shift perturbations (CSPs) were calculated from ^{1}H and ^{15}N chemical shift differences between protein solutions with and without KCl according to the equation $\sqrt{\Delta\delta_H^2 + (0.14 \cdot \Delta\delta_N^2)}$.

[^{15}N, ^{1}H] Heteronuclear Nuclear Overhauser Effect

Steady-state [^{15}N, ^{1}H] heteronuclear nuclear Overhauser effect (hetNOE) measurements were carried out for 4 protein samples (see Tables S1 and S2) with and without proton saturation during the relaxation delay. Either 5 s of relaxation delay and 3 s of proton saturation, or 8 s of relaxation delay without successive proton saturation were used. The heteronuclear NOE values were determined as ratios of peak intensities measured from spectra acquired with and without proton saturation. NMR spectra were processed using Bruker TopSpin 4.0.8 and analyzed using CCPN.[51] hetNOE values were determined as intensity ratios between spectra with and without proton saturation. For estimation of intensity errors, 10 randomly distributed noise peaks were picked in both spectra and the absolute intensity values were averaged. Errors of hetNOE values were calculated using error propagation assuming that the distributions underlying all data are normally distributed.

^{15}N Relaxation Dispersion

Constant-time ^{15}N-CPMG (CT-CPMG) relaxation dispersion experiments[52] were measured for all four protein samples (experimental details summarized in Table 1). Experiments were performed with a constant-time delay as mentioned in Table 1 for different protein samples. Nine variable CPMG frequencies (ν_{CPMG}) ranging from 50 Hz to 2000 Hz were collected. Besides, for each dataset the frequencies 50 Hz and 750 Hz were repeated for estimation of the error in $R_{2,eff}$, and a reference spectrum without constant time delay ($T_{CPMG} = 0$) was recorded. For each 2D dataset corresponding to one CPMG frequency, 128 and 2048 complex points in the indirect and direct dimensions, respectively, were collected with 32 scans. 2D datasets for all frequencies were measured in a scan-interleaved fashion. A recycle delay of 1.5 s was used, giving rise to a net acquisition time between 15 h and 52 h per sample. NMR relaxation data were processed using Topspin 4.0.8. Peak intensities were quantified and visualized with CCPN.[51] The effective amide ^{15}N transverse relaxation rate at each CPMG frequency was calculated according to the relation of effective transverse relaxation rate ($R_{2,eff}$),

$$R_{2,\mathrm{eff}} = -\frac{1}{t} \cdot \ln\left(\frac{I}{I_0}\right) \tag{4}$$

where I is the peak intensity, I_0 is the reference peak intensity of a spectrum recorded without CT-CPMG relaxation period, and t is a constant time delay.

Evaluation of CPMG data was performed using ChemEx.[53] Relaxation dispersion curves were fitted analytically according to the Bloch-McConnell equations on the basis of a two-state exchange model. Errors were estimated from the duplicate points measured for 50 Hz and 750 Hz field strength. The exchange contribution to the exchange rate R_{ex} was determined as the difference between the maximum calculated effective transverse relaxation rate $R_{2,eff}$ (maximum of the fit curve) and the fitted intrinsic transverse relaxation rate R_2^0.

Table 1. Conditions of hetNOE and CPMG experiments.

	SH3	Ubiquitin	hCAII	MBP
T_{CPMG} (ms)	80	80	40	30
δ_{O1P} (ppm)	116.0	116.0	116.0	119.0
PW_{90} without KCl (μs)	7.30	7.19	7.35	7.10
PW_{90} with KCl (μs)	9.47	10.12	13.36	15.23

Evaluation of hetNOE and R_{ex} Values

Sequential hetNOE and R_{ex} plots, histograms and box plots were generated using the Matplotlib module of Python 3; the sequential secondary structure representations on top of the plots were generated using the Biotite module of Python 3. To better identify differences in behavior between different secondary structure elements, hetNOE and CPMG values were grouped into three secondary-structure classes (sheet, helix and coil) and normalized for each secondary-structure class. Secondary-structure elements were determined based on the X-ray structures with PDB ID 2NUZ, 1UBQ, 2CBA and 1ANF using DSSP[54] and grouped into three instead of the default eight DSSP secondary structure types (3-, 4- and 5-turn helices (G, H and I) as helix; extended strands in β-sheet conformation (B) and residues in isolated β-bridges (E) as sheet; bends (S), hydrogen bonded turns (T) and unstructured regions (U) as coil).

Simulation Methods

We used the TIP3P water model,[55] the AMBER ff14SB[56,57] force field for proteins and the potassium and chloride parameters of Joung and Cheatham[58] for TIP3P water. The Lennard-Jones (LJ) parameters for interactions involving carboxylate groups were modified from the default values obtained using combination rules. The self-interaction LJ parameters for all carboxylate oxygen atoms use the values derived by Kashefolgheta et al.,[59] which approximate the hydration free energy of acetate in TIP3P water better than the original AMBER parameters. The LJ parameters for the interaction between carboxylate and the side chain of the positively charged amino acid lysine were also modified,[59] thus avoiding unphysically strong salt bridges. The LJ parameters for the interaction between carboxylate groups and potassium were modified to improve the solution activity derivative and the carboxylate-potassium distance

in a protein crystal.[60] The modified parameter values are given in section S1.3.1. The $[2Fe\text{-}2S]^{2+}$ ligand present in the ferredoxin proteins was simulated using the parameters developed by Carvalho et al.[61] for the [2Fe-2S] ferredoxin from *Mastigocladus laminosus*, with some modifications: i) The equilibrium angles in our simulations are those in the crystal structure of our proteins. ii) the force constant for the Fe-S-C angle, missing in the parameter set of Carvalho et al. for the $[2Fe\text{-}2S]^{2+}$ from *Mastigocladus laminosus*, is given the value for the desulforedoxin protein from *Desulfovibrio gigas*.[61] This change is acceptable because the ferredoxins studied here contains Fe(III) coordinated by four cysteines in the same configuration as those in the desulforedoxin protein. The zinc metal center of the carbonic anhydrase proteins is connected to three histidine residues and one water molecule. That metal center was simulated using ZAFF (Zinc AMBER force field)[62,63] and the van der Waals (vdW) parameters for the zinc ion from Li et al.[63]

Simulations were performed using the GPU version of the pmemd engine in AMBER 2018.[64] Only the l-bfgs minimization step was performed on the Sander engine of AMBER 2018 because it was not available in the pmemd engine. Each protein was simulated at $b_{KCl} = 0.15\ mol\,kg^{-1}$ and $b_{KCl} = 2\ mol\,kg^{-1}$. The simulation boxes are cubic and have edge lengths of ≈ 100 Å; the minimum distance between the protein surface and the box face was ≈ 20 Å. Periodic boundary conditions were applied in all directions. The SHAKE[65] algorithm was used to constrain all bonds with hydrogen atoms. A 1 fs time step was used to simulate the carbonic anhydrase proteins because of the water molecule that coordinates the zinc metal center, whereas a 2 fs time step was used for all other simulations. A Langevin thermostat with a collision frequency of $0.01\ ps^{-1}$ was used to keep the average system temperature at 298 K. This low collision frequency was necessary to reduce the impact of the thermostat on the dynamics of the system, and was sufficient to stabilize the average temperature. This low collision frequency ensures that the self-diffusivity, rotational correlation time, and shear viscosity stay within 2% of those obtained from *NVE* simulations at the same temperature.[66] The production simulations were done in the NVT ensemble and lasted 0.5 μs for carbonic anhydrase and 1 μs for all other proteins, with configurations saved every 100 ps for analysis. Further simulation details can be found in section S1.3.2 and in our prior publication.[60] These simulations were previously analysed to understand the structure and dynamics of the protein solvation shells; those results are reported in that prior publication.[60] Here we focus exclusively on the dynamics of the protein.

Protein conformational dynamics was characterized in simulations by calculating the root mean square fluctuations (RMSF) and the hydrophobic surface area (SASA) as a function of time. This analysis was done with the software packages VMD[67] and Cpptraj package[68] from Amber software. The median protein structure was calculated using the software package Theseus.[69,70] Details of these calculations can be found in section S1.3.

Acknowledgements

Funded by the Deutsche Forschungsgemeinschaft (DFG, German Research Foundation) under: Germany's Excellence Strategy – EXC 2033 – 390677874 – RESOLV; grant 325871075 and the Emmy Noether program (to R.L.); grant 639429 (to A.V.V.). A.V.V. gratefully acknowledges Lothar Brendel and Florian Führer for helpful discussions. Open Access funding enabled and organized by Projekt DEAL.

Conflict of Interests

The authors have no conflict of interest to report.

Data Availability Statement

The data that support the findings of this study are available from the corresponding author upon reasonable request.

Keywords: biological activity · molecular dynamics · protein models · protein modifications · salt effect

[1] J. K. Lanyi, *Bacteriol. Rev.* **1974**, *38*, 272.
[2] J. Peters, R. Oliva, A. Caliò, P. Oger, R. Winter, *Chem. Rev.* **2023**, 10.1021/acs.chemrev.3c00432.
[3] C. Brininger, S. Spradlin, L. Cobani, C. Evilia, *Semin. Cell Dev. Biol.* **2018**, *84*, 158.
[4] P. M. Tessier, A. M. Lenhoff, *Curr. Opin. Biotechnol.* **2003**, *14*, 512 .
[5] A. C. Dumetz, A. M. Snellinger-O'Brien, E. W. Kaler, A. M. Lenhoff, *Protein Sci.* **2007**, *16*, 1867.
[6] B. Guo, S. Kao, H. McDonald, A. Asanov, L. Combs, W. William Wilson, *J. Cryst. Growth* **1999**, *196*, 424 .
[7] G. Graziano, A. Merlino, *Biochim. Biophys. Acta Proteins Proteomics* **2014**, *1844*, 850.
[8] S. P. Kennedy, W. V. Ng, S. L. Salzberg, L. Hood, S. DasSarma, *Genome Res.* **2001**, *11*, 1641.
[9] S. Paul, S. K. Bag, S. Das, E. T. Harvill, C. Dutta, *Genome Biol.* **2008**, *9*, R70.
[10] A. Siglioccolo, A. Paiardini, M. Piscitelli, S. Pascarella, *BMC Struct. Biol.* **2011**, *11*, 50.
[11] D. Madern, G. Zaccai, *Biochimie* **2004**, *86*, 295.
[12] M. S. Date, B. N. Dominy, *Commun. Comput. Phys.* **2013**, *13*, 90.
[13] P. A. Fields, *Comp. Biochem. Physiol. Part A* **2001**, *129*, 417.
[14] K. Teilum, J. G. Olsen, B. B. Kragelund, *Biochim. Biophys. Acta Proteins Proteomics* **2011**, *1814*, 969.
[15] P. Arroyo-Manez, D. E. Bikiel, L. Boechi, L. Capece, S. D. Lelia, D. A. Estrin, M. A. Marti, D. M. Moreno, A. D. Nadra, A. A. Petruk, *Biochim. Biophys. Acta Proteins Proteomics* **2011**, *1814*, 1054.
[16] E. Z. Eisenmesser, O. Millet, W. Labeikovsky, D. M. Korzhnev, M. Wolf-Watz, D. A. Bosco, J. J. Skalicky, L. E. Kay, D. Kern, *Nature* **2005**, *438*, 117.
[17] L. Y. P. Luk, E. J. Loveridge, R. K. Allemann, *Phys. Chem. Chem. Phys.* **2015**, *17*, 30817.
[18] P. H. Wang, R. B. Best, J. Blumberger, *J. Am. Chem. Soc.* **2011**, *133*, 3548.
[19] M. Mevarech, F. Frolow, L. M. Gloss, *Biophys. Chem.* **2000**, *86*, 155.
[20] F. Ferrage, D. Cowburn, R. Ghose, *J. Am. Chem. Soc.* **2009**, *131*, 6048.
[21] M. Wong, G. Khirich, J. P. Loria, *Biochemistry* **2013**, *52*, 6548.
[22] M. Wong, G. Khirich, J. P. Loria, *Biochemistry* **2013**, *52*, 7160.
[23] B. Mateos, O. Millet, *J. Magn. Reson. Open* **2022**, *12–13*, 100072.
[24] Q. Li, M. Li, C. Li, X. Li, C. Lu, X. Tu, Z. Zhang, X. Zhang, *FEBS Lett.* **2021**, *595*, 521.
[25] M. Tehei, D. Madern, C. Pfister, G. Zaccai, *Proc. Natl. Acad. Sci. USA* **2001**, *98*, 14356.
[26] B. Hess, N. F. A. van der Vegt, *Proc. Natl. Acad. Sci. USA* **2009**, *106*, 13296.
[27] D. Sitkoff, K. A. Sharp, B. Honig, *Biophys. Chem.* **1994**, *51*, 397.
[28] K. A. Sharp, A. Nicholls, R. F. Fine, B. Honig, *Science* **1991**, *252*, 106.
[29] K. Ali, A.-H. Shah, S. Bilal, A.-U.-H. Shah, *Colloids Surf. A* **2009**, *337*, 194.
[30] J. H. Roh, M. Tyagi, P. Aich, K. Kim, R. M. Briber, S. A. Woodson, *Soft Matter* **2015**, *11*, 8741.
[31] J. Roh, *Macromol. Chem. Phys.* **2016**, *217*, 256.
[32] G. Zaccai, F. Cendrin, Y. Haik, N. Borochov, H. Eisenberg, *J. Mol. Biol.* **1989**, *208*, 491.
[33] X. Tadeo, B. López-Méndez, T. Trigueros, A. Laín, D. Castaño, O. Millet, *PLoS Biol.* **2009**, *7*, e1000257.
[34] D. Madern, C. Ebel, G. Zaccai, *Extremophiles* **2000**, *4*, 91.
[35] G. Ortega, T. Diercks, O. Millet, *Chem. Biol.* **2015**, *22*, 1597.
[36] P. Herrero, A. Pejenaute, O. Millet, G. Ortega, *bioRxiv* **2024**, page 2024.01.08.574673.
[37] H. Geraili, A. V. Verde, *Biophys. J.* **2023**, *122*, 2577.
[38] A. H. Elcock, J. A. McCammon, *J. Mol. Biol.* **1998**, *280*, 731.

[39] F. Frolow, M. Harel, J. L. Sussman, M. Mevarech, M. Shoham, *Nat. Struct. Mol. Biol.* **1996**, *3*, 452.
[40] R. Deole, J. Challacombe, D. W. Raiford, W. D. Hoff, *J. Biol. Chem.* **2013**, *288*, 581.
[41] G. Janson, G. Valdes-Garcia, L. Heo, M. Feig, *Nat. Commun.* **2023**, *14*, 774.
[42] G. E. Karniadakis, I. G. Kevrekidis, L. Lu, P. Perdikaris, S. Wang, L. Yang, *Nat. Rev. Phys.* **2021**, *3*, 422.
[43] G. K. Meghwanshi, N. Kaur, S. Verma, N. K. Dabi, A. Vashishtha, P. D. Charan, P. Purohit, H. S. Bhandari, N. Bhojak, R. Kumar, *Biotechnol. Appl. Biochem.* **2020**, *67*, 586.
[44] G. Rossino, M. S. Robescu, E. Licastro, C. Tedesco, I. Martello, L. Maffei, G. Vincenti, T. Bavaro, S. Collina, *Chirality* **2022**, *34*, 1403.
[45] S. J. Horn, G. Vaaje-Kolstad, B. Westereng, V. Eijsink, *Biotechnol. Biofuels* **2012**, *5*, 45.
[46] A. Bangaru, A. Kamasani, C. Kruthiventi, M. Banala, V. Shreya, Y. Vineetha, A. Shalini, B. Mishra, R. Yadavalli, C. Kuppam, C. Nagendranatha Reddy, Role of Enzymes in Biofuel Production: Recent Developments and Challenges, in P. Chowdhary, N. Khanna, S. Pandit, R. Kumar (Editors), *Bio-clean energy technologies: Vol. 1*, pages 81–112, Springer Nature Singapore, Singapore **2022**.
[47] I. Dundas, *Extremophiles* **1998**, *2*, 375.
[48] B. M. Rode, *Peptides* **1999**, *20*, 773.
[49] L. M. Longo, J. Lee, M. Blaber, *Proc. Natl. Acad. Sci. USA* **2013**, *110*, 2135.
[50] L. Longo, M. Blaber, *Front. Microbiol.* **2014**, *4*, 418.
[51] W. F. Vranken, W. Boucher, T. J. Stevens, R. H. Fogh, A. Pajon, M. Llinas, E. L. Ulrich, J. L. Markley, J. Ionides, E. D. Laue, *Proteins* **2005**, *59*, 687.
[52] J. P. Loria, M. Rance, A. G. Palmer, *J. Am. Chem. Soc.* **1999**, *121*, 2331.
[53] G. Bouvignies, ChemEx.
[54] W. Kabsch, C. Sander, *Biopolymers* **1983**, *22*, 2577.
[55] W. L. Jorgensen, J. Chandrasekhar, J. D. Madura, R. W. Impey, M. L. Klein, *J. Chem. Phys.* **1983**, *79*, 926.
[56] W. D. Cornell, P. Cieplak, C. I. Bayly, I. R. Gould, K. M. Merz, D. M. Ferguson, D. C. Spellmeyer, T. Fox, J. W. Caldwell, P. A. Kollman, *J. Am. Chem. Soc.* **1995**, *117*, 5179.
[57] J. A. Maier, C. Martinez, K. Kasavajhala, L. Wickstrom, K. E. Hauser, C. Simmerling, *J. Chem. Theory Comput.* **2015**, *11*, 3696.
[58] I. S. Joung, T. E. Cheatham, *J. Phys. Chem. B* **2008**, *112*, 9020.
[59] S. Kashefolgheta, A. Vila Verde, *Phys. Chem. Chem. Phys.* **2017**, *19*, 20593.
[60] H. Geraili Daronkola, A. Vila Verde, *Biophys. J.* **2021**, *120*, 2746.
[61] A. T. P. Carvalho, A. F. S. Teixeira, M. J. Ramos, *J. Comput. Chem.* **2013**, *34*, 1540.
[62] M. B. Peters, Y. Yang, B. Wang, L. Füsti-Molnár, M. N. Weaver, K. M. Merz, *J. Chem. Theory Comput.* **2010**, *6*, 2935.
[63] P. Li, B. P. Roberts, D. K. Chakravorty, K. M. Merz, *J. Chem. Theory Comput.* **2013**, *9*, 2733.
[64] D. Case, I. Ben-Shalom, S. Brozell, D. Cerutti, T. Cheatham III, V. Cruzeiro, T. Darden, R. Duke, D. Ghoreishi, M. Gilson, H. Gohlke, A. Goetz, D. Greene, R. Harris, N. Homeyer, Y. Huang, S. Izadi, A. Kovalenko, T. Kurtzman, T. Lee, S. LeGrand, P. Li, C. Lin, J. Liu, T. Luchko, R. Luo, D. Mermelstein, K. Merz, Y. Miao, G. Monard, C. Nguyen, H. Nguyen, I. Omelyan, A. Onufriev, F. Pan, R. Qi, D. Roe, A. Roitberg, C. Sagui, S. Schott-Verdugo, J. Shen, C. Simmerling, J. Smith, R. Salomon-Ferrer, J. Swails, R. Walker, J. Wang, H. Wei, R. Wolf, X. Wu, L. Xiao, D. York, P. Kollman, *Amber 18*, University of California, San Francisco **2018**.
[65] J.-P. Ryckaert, G. Ciccotti, H. J. C. Berendsen, *J. Comput. Phys.* **1977**, *23*, 321.
[66] J. E. Basconi, M. R. Shirts, *J. Chem. Theory Comput.* **2013**, *9*, 2887.
[67] W. Humphrey, A. Dalke, K. Schulten, *J. Mol. Graphics* **1996**, *14*, 33.
[68] D. R. Roe, T. E. I. Cheatham, *J. Chem. Theory Comput.* **2013**, *9*, 3084.
[69] D. L. Theobald, P. A. Steindel, *Bioinformatics* **2012**, *28*, 1972.
[70] D. L. Theobald, D. S. Wuttke, *PLoS Comput. Biol.* **2008**, *4*, e43.

Manuscript received: January 24, 2024
Revised manuscript received: February 20, 2024
Accepted manuscript online: February 23, 2024
Version of record online: May 16, 2024